

Self-organized pattern synchronization modulated by stochasticity in coupled plankton ecosystems

Ju Kang¹, Yiyuan Niu², Yuanzhi Li¹, Quan-Xing Liu³, Chengjin Chu^{1,*}

¹School of Ecology, Sun Yat-sen University, Shenzhen 518107, China

²School of Physics, Sun Yat-sen University, Guangzhou 510275, China

³School of Mathematical Sciences, Shanghai Jiao Tong University, Shanghai 200240, China

*Corresponding author: chuchjin@mail.sysu.edu.cn

Abstract

Spatial patterning and synchronization are pervasive features of plankton communities, yet the mechanisms that allow such patterns to persist coherently under environmental noise remain unresolved. In vertically structured aquatic ecosystems, plankton populations are often organized into distinct layers, raising the question of how interactions between layers shape both spatial self-organization and robustness. Here, we develop a spatiotemporal ecosystem model of a two-layer plankton community to examine the role of passive diffusive coupling under stochastic environmental fluctuations. We show that interlayer diffusion induces a sharp transition from independent, layer-specific Turing patterns to fully synchronized spatial patterns once the coupling strength exceeds a critical threshold. Importantly, the same coupling mechanism markedly enhances the stability of spatial patterns against environmental noise, extending their persistence far beyond that of non-coupled layers. Moreover, we uncover a trophic hierarchy in noise sensitivity, with zooplankton exhibiting substantially greater vulnerability than phytoplankton. Together, these results identify passive diffusive coupling as a unifying mechanism that simultaneously promotes spatial synchronization and robustness, providing a mechanistic explanation for the persistence of coherent plankton patterns in fluctuating aquatic environments.

Keywords: Self-organized patterns, reaction-diffusion model, synchronous dynamics, Monte Carlo simulation, environmental noise

1. Introduction

Spatial pattern formation is a pervasive and striking feature of plankton communities in aquatic ecosystems, manifesting as patchy distributions across both horizontal and vertical dimensions. Such spatial heterogeneity has been widely documented in field observations and experiments and is thought to play a central role in regulating species interactions, ecosystem functioning, and biogeochemical cycling [1–5]. Understanding the mechanisms that generate and sustain these patterns has therefore long been a central objective in aquatic ecology.

Over the past decades, a broad range of biological and physical processes, including predation, migration, diffusion, turbulence, and hydrodynamic forcing, have been proposed as drivers of plankton spatial self-organization [6–15]. Many of these mechanisms are capable of producing self-organized spatial patterns in idealized settings, particularly within single layers or effectively isolated spatial domains. Recent experimental studies have further revealed that stochasticity intrinsic to biological systems can itself drive Turing-like pattern formation, as demonstrated in synthetic bacterial populations [16] and in the development of trichomes in *Arabidopsis* leaves [17]. However, most existing studies, whether focused on ecological or molecular systems, have concentrated on pattern formation in isolation within single-layer or isolated domains, rather than on the persistence and coherence of patterns in realistic environments where multiple spatial domains are dynamically coupled and continuously exposed to environmental fluctuations continuously exposed to environmental fluctuations.

In aquatic environments, this discriminatory capacity is frequently observed in their selective feeding on toxic versus non-toxic phytoplankton species [18, 19]. Such avoidance is not always absolute; under conditions of limited resources, some zooplankton initially prefer non-toxic prey but gradually shift to toxic alternatives when necessary [18, 19]. This flexible foraging strategy implies that prey quality, including toxicity, can at times override established selection criteria such as size. For example, *Artemia salina* has been shown to prefer larger non-toxic prey over smaller toxic ones [20]. Thus, nuanced avoidance behavior can significantly influence population persistence and community structure. Toxic prey avoidance in zooplankton is shaped more strongly by behavioral adaptation than by physiological resistance [21]. Although physiological tolerance to toxins may evolve over time [22–24], behavioral strategies such as selective ingestion

often constitute the primary defense mechanism [25, 26]. Phytoplankton-released toxins can serve as a defense against grazing [21, 27] and may also negatively affect competing species [28, 29]. These toxins exert a range of adverse effects on zooplankton, from deterring feeding to impairing physiological function and reducing reproductive success [21, 30, 31]. The intensity of zooplankton avoidance behavior, which varies with the availability of non-toxic prey, is therefore a key factor influencing species coexistence, ecosystem stability, and potential harmful algal bloom formation, as indicated by modeling studies [32].

Vertical structuring is a ubiquitous characteristic of aquatic systems. Stratification of the water column, together with active vertical migration of zooplankton and passive transport of phytoplankton, naturally couples plankton communities across depth layers [12, 33–40]. Such coupling establishes an extended ecosystem in which biological and physical processes in one layer can influence pattern dynamics in another. Notable examples include euphausiids (e.g., *Euphausia mucronata*) and the semi-pelagic squat lobster *Pleuroncodes monodon* in the Peruvian upwelling system, which undertake diel vertical migrations connecting surface and deep waters, thereby actively linking biogeochemical processes across depth layers [40]. Empirical and theoretical studies have suggested that vertical coupling may promote synchronization of spatial patterns across layers [7–9, 33, 41–43]. Despite this extensive body of work, most existing studies have focused on pattern formation within single layers or under effectively isolated spatial domains, often by isolating individual biological processes or physical drivers [9–11]. However, the mechanisms by which vertically coupled plankton systems achieve and maintain synchronized spatial self-organization remain incompletely understood [44].

This gap becomes particularly pronounced in the presence of environmental stochasticity. Aquatic ecosystems are inherently noisy, with fluctuating physical conditions such as turbulence, nutrient supply, and hydrodynamic forcing acting as persistent sources of perturbation. In reaction-diffusion systems, stochasticity is generally expected to disrupt self-organized spatial patterns. Nonetheless, coherent and synchronized plankton patterns are frequently observed in nature, even under highly variable environmental conditions. How vertically coupled plankton communities reconcile this apparent tension between noise-induced disruption and persistent spatial coherence remains an open and fundamental problem.

In this work, we address this problem by developing a spatiotemporal ecosystem model of a two-layer plankton community coupled through passive diffusive exchange. By deliberately focusing on physical coupling rather than species-specific behavioral complexity, we isolate the role of diffusion in shaping spatial dynamics under stochastic perturbations. We show that increasing coupling strength induces a sharp transition from independent, layer-specific Turing patterns to fully synchronized spatial patterns once a critical threshold is exceeded. Importantly, the same diffusive coupling mechanism substantially enhances the robustness of spatial patterns against environmental noise, allowing synchronized structures to persist far beyond the regime where non-coupled layers lose coherence. Furthermore, we find that noise sensitivity differs systematically across trophic levels, with zooplankton populations exhibiting greater vulnerability than phytoplankton. Together, these results identify passive diffusive coupling as a core mechanism that simultaneously promotes spatial synchronization and robustness, offering a mechanistic explanation for the persistence of coherent plankton patterns in fluctuating aquatic environments.

2. Results

2.1. A coupled two-layer reaction-diffusion framework

In stratified water columns, the number of coupled plankton systems is determined by the number of vertical layers. A greater number of layers leads to more intricate dynamic patterns in the coupled system, making it more challenging to decipher the underlying nonlinear self-organization mechanisms. The degree of stratification, both in terms of the number of layers and the strength of gradients, shapes the physical template upon which biological self-organization occurs. Importantly, stratification does not imply the absence of turbulence; rather, it modulates turbulent processes that may serve as sources of environmental stochasticity. These stochastic disturbances, in turn, interact with the deterministic dynamics of pattern formation, potentially influencing the stability and synchronization of spatial structures across layers. Therefore, to focus on the core mechanisms, namely Turing instability, diffusive coupling, and their interplay with environmental stochasticity, this study analyzes the simplest case of two-layer stratification, an ecologically realistic scenario where two subsystems, each comprising non-toxic phytoplankton, toxic phytoplankton, and zooplankton,

are diffusively coupled. Building on this two-layer model, we analyze a vertically stratified planktonic ecosystem using coupled reaction–diffusion equations that resolve horizontal spatial structure within two vertically distinct layers. The model retains three state variables per layer: non-toxic phytoplankton $N_i(x, y, t)$, toxic phytoplankton $T_i(x, y, t)$ and zooplankton $Z_i(x, y, t)$ for layer index $i \in \{1, 2\}$. In natural aquatic ecosystems, non-toxic phytoplankton (N_i) primarily corresponds to green algae (e.g., *Chlorella*, *Scenedesmus*) and diatoms, which serve as high-quality food sources for zooplankton. Toxic phytoplankton (T_i) corresponds to cyanobacteria (e.g., *Microcystis aeruginosa*, *Raphidiopsis raciborskii*), which produce microcystins that adversely affect zooplankton feeding, growth, and reproduction. Zooplankton (Z_i) encompasses functional groups such as copepods (e.g., *Mesocyclops*, *Eudiaptomus*) and cladocerans (e.g., *Daphnia*, *Moina*), which exhibit different feeding selectivities—copepods are capable of selective feeding based on food quality, whereas cladocerans are non-selective filter-feeders. These grazers play a pivotal role in linking primary producers to higher trophic levels and regulating phytoplankton community structure through top-down control. Each layer occupies a square domain $\Omega = [0, L] \times [0, L] \subset \mathbb{R}^2$ with smooth boundary $\partial\Omega$; homogeneous Neumann (no-flux) boundary conditions are imposed on all species (see below). The model of two coupled non-toxic phytoplankton, toxic phytoplankton and zooplankton well-mixed system can be written as follows:

$$\left\{ \begin{array}{l} \frac{\partial N_1(x,y,t)}{\partial t} = f_1(N_1, T_1, Z_1) + d_{11}\Delta N_1 + h_{11}(N_2 - N_1), \\ \frac{\partial T_1(x,y,t)}{\partial t} = g_1(N_1, T_1, Z_1) + d_{12}\Delta T_1 + h_{12}(T_2 - T_1), \\ \frac{\partial Z_1(x,y,t)}{\partial t} = \varphi_1(N_1, T_1, Z_1) + d_{13}\Delta Z_1 + d_{31}Z_1\Delta N_1 - d_{32}Z_1\Delta T_1 + h_{13}(Z_2 - Z_1), \\ \frac{\partial N_2(x,y,t)}{\partial t} = f_2(N_2, T_2, Z_2) + d_{21}\Delta N_2 + h_{21}(N_1 - N_2), \\ \frac{\partial T_2(x,y,t)}{\partial t} = g_2(N_2, T_2, Z_2) + d_{22}\Delta T_2 + h_{22}(T_1 - T_2), \\ \frac{\partial Z_2(x,y,t)}{\partial t} = \varphi_2(N_2, T_2, Z_2) + d_{23}\Delta Z_2 + d_{41}Z_2\Delta N_2 - d_{42}Z_2\Delta T_2 + h_{23}(Z_1 - Z_2), \\ \frac{\partial N_i(x,y,t)}{\partial n} = \frac{\partial T_i(x,y,t)}{\partial n} = \frac{\partial Z_i(x,y,t)}{\partial n} = 0, i = 1, 2, (x, y) \in \partial\Omega, \\ N_i(x, y, t) > 0, T_i(x, y, t) > 0, Z_i(x, y, t) > 0, t > 0, (x, y) \in \Omega. \end{array} \right. \quad (1)$$

where $\Delta = \frac{\partial^2}{\partial x^2} + \frac{\partial^2}{\partial y^2}$ and ∂_n denotes the outward normal derivative on $\partial\Omega$. The coefficients d_{ij} with $i \in \{1, 2\}$ and $j \in \{1, 2, 3\}$ denote species-specific diffusion coefficients for N_i , T_i and Z_i respectively; coefficients denoted d_{31} , d_{32} , d_{41} , d_{42} represent cross-diffusion couplings between zooplankton and phytoplankton. The linear exchange terms with rates h_{ij} model vertical migration between layers for each species; unless otherwise stated, we assume $h_{il} = h$ for convenience. The reaction terms employed here are Holling-type functional responses f_i , g_i and φ_i for zooplankton grazing [6, 45]:

$$\left\{ \begin{array}{l} f_i(N_i, T_i, Z_i) = r_{i1}N_i \left(1 - \frac{N_i + \alpha_{i1}T_i}{K_{i1}} \right) - \frac{w_{i1}N_iZ_i}{p_{i1} + N_i}, \\ g_i(N_i, T_i, Z_i) = r_{i2}T_i \left(1 - \frac{T_i + \alpha_{i2}N_i}{K_{i2}} \right) - \frac{w_{i2}T_iZ_i}{p_{i2} + T_i + \beta_i N_i}, \\ \varphi_i(N_i, T_i, Z_i) = \frac{c_{i1}w_{i1}N_iZ_i}{p_{i1} + N_i} - \frac{c_{i2}w_{i2}T_iZ_i}{p_{i2} + T_i + \beta_i N_i} - m_i Z_i. \end{array} \right. \quad (2)$$

where r_{i1} and r_{i2} ($i = 1, 2$) denote the constant intrinsic growth rates of N_i and T_i , respectively; K_{i1} and K_{i2} denote the carrying capacities of N_i and T_i , respectively; α_{i1} and α_{i2} measure the competitive effect of T_i on N_i , and N_i on T_i , respectively; w_{i1} and w_{i2} represent the rates at which N_i , T_i are consumed by Z_i , respectively; p_{i1} and p_{i2} denote half saturation constants for N_i and T_i , respectively; c_{i1} and c_{i2} represent the conversion rates of N_i to Z_i and T_i to Z_i , respectively; β_i denotes the intensity of avoidance of T_i by Z_i , in the presence of N_i ; m_i denotes the mortality rate of the zooplankton Z_i . Note that the model assumes gradient exchange between upper and bottom layer. This may not reflect a realistic ecosystem but a idea framework to address the question on how spatial couple effect the species coexistence and spatial distribution.

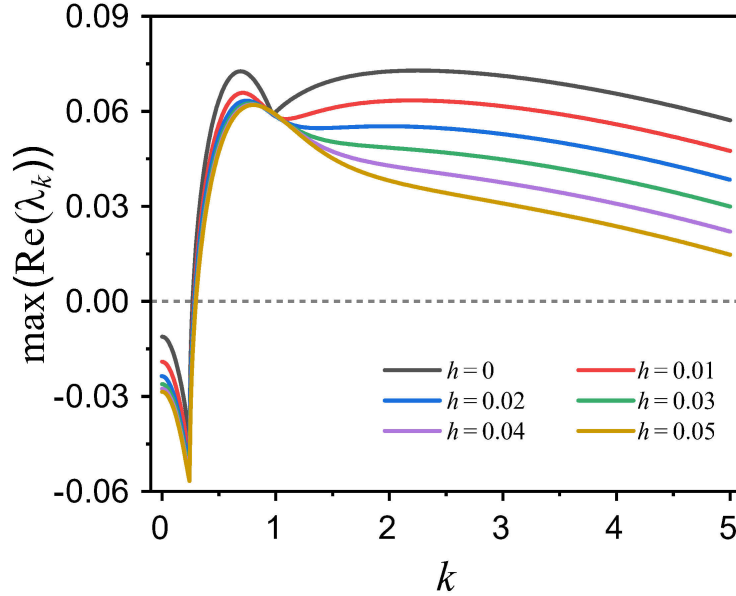


Figure 1: Theoretical dispersion relation: maximum real part of eigenvalues $\max(\text{Re}(\lambda_k))$ as a function of horizontal wavenumber k for representative vertical exchange rates h . Curves correspond to parameter sets in Table 1 of the Supplementary Materials (SM).

2.2. Independent pattern formation in the non-coupled system

We first analyze the non-coupled case (see Fig. 1 for $h = 0$), which serves as a reference regime for understanding the intrinsic pattern-forming tendencies of each layer. Uniform steady states are obtained by setting all temporal and spatial derivatives to zero, yielding a coexistence equilibrium $E^* = (N_1^*, T_1^*, Z_1^*, N_2^*, T_2^*, Z_2^*)$ in which all species persist in both layers. Linear stability analysis around E^* leads to a dispersion relation $\max(\text{Re}(\lambda_k))$ across a range of wavenumber k . For each k , six eigenvalues arise from the linearized system, reflecting the three-species dynamics in two non-coupled layers (see Supplementary Materials (SM) I for details). According to Turing instability theory [46–49], spatial patterning occurs when $\max(\text{Re}(\lambda_k)) > 0$ for some $k > 0$.

In the absence of coupling, the dispersion relation exhibits two distinct peaks (Fig. 1, $h = 0$), each corresponding to a critical Turing mode localized in each layer. This double-peak structure indicates that both layers independently satisfy the conditions for diffusion-driven instability, but with different preferred spatial scales. Numerical simulations confirm this prediction: the upper (layer 1) and lower (layer 2) layers develop self-organized patterns with distinct spatial structures, including spots, stripes, and mixed forms (Figs. 2, S1). These differences arise from layer-specific parameter values, such as diffusion coefficients and interaction strengths, which selectively amplify different instability modes. The non-coupled system therefore supports independent pattern formation in each layer, without any tendency toward spatial synchronization.

2.3. Coupling-induced synchronization of spatial patterns

Introducing inter-layer coupling fundamentally alters the pattern-forming dynamics. As the coupling strength h increases from zero, the two initially separated peaks in the dispersion relation gradually approach each other and eventually merge into a single dominant peak (see Fig. 1, $h > 0$). This transition indicates that the previously independent Turing modes become dynamically linked through vertical migration. The simulations confirm this dynamical shift, as the initially asynchronous layers evolve toward a state of synchronized spatial patterns (see Figs. 3, S2). Patterns that were distinct in the non-coupled regime evolve into spatially coherent structures sharing the same dominant wavelength and morphology. This synchronization reflects the locking of pattern-forming modes between layers, driven by sufficient inter-layer exchange.

The synchronization transition is quantified by defining the synchronization errors as $\delta N = |N_1 - N_2|$, $\delta T = |T_1 - T_2|$, and $\delta Z = |Z_1 - Z_2|$. In the non-coupled regime, these errors remain large and fluctuate around elevated

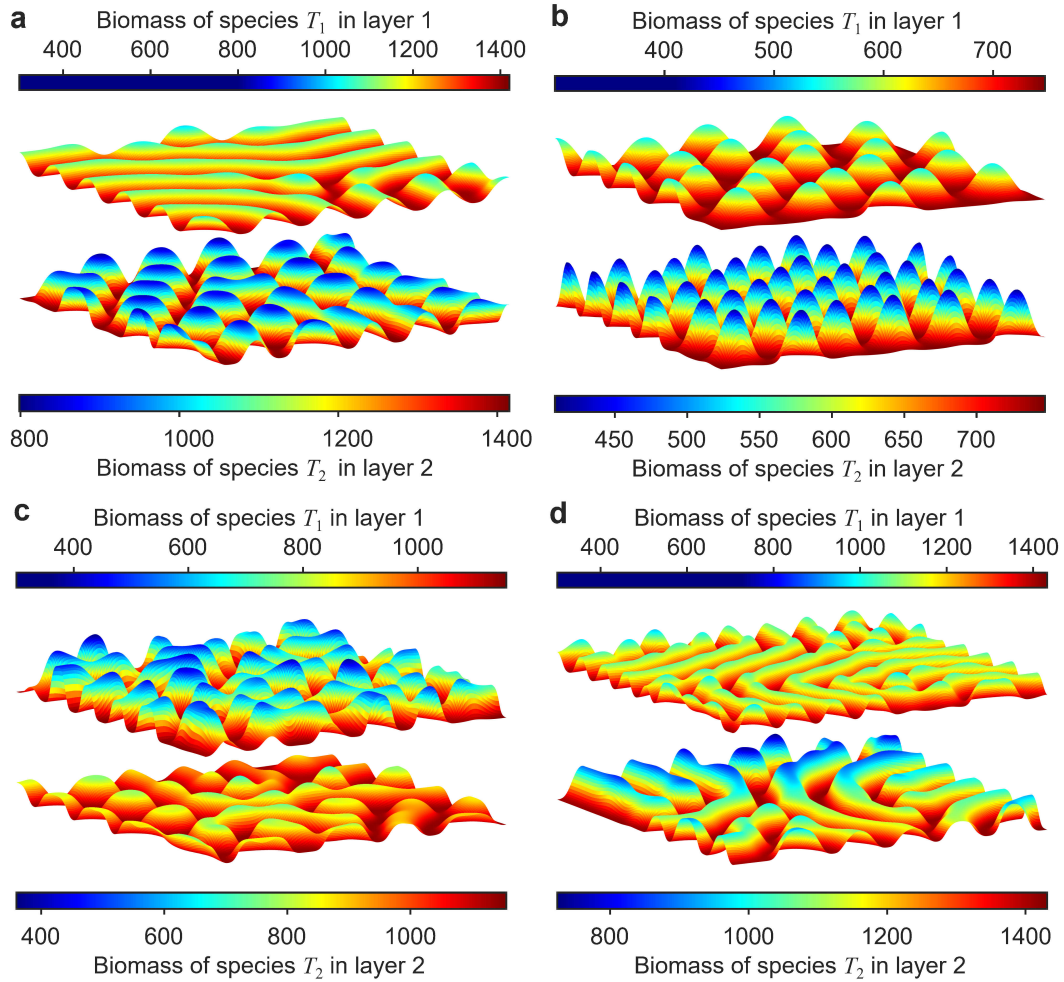


Figure 2: Self-organized pattern dynamics in the non-coupled aquatic system (without vertical migration, $h = 0$). (a-d) Spatial patterns in the surface (*layer 1*) and bottom (*layer 2*) layers exhibit distinct structural forms. Under different parameter sets but identical initial conditions, the system exhibits a variety of coexisting spatial configurations, each with distinct pattern types in the two *layers*: (a) stripes in *layer 1* and spots in *layer 2*, (b) spots in both *layers*, (c) mixed patterns in both *layers*, and (d) stripes in both *layers*. The dispersion relation corresponding to the case in (a) is shown in Fig. 1; panels (b-d) exhibit analogous dispersion behaviour (not shown). The spatial pattern structures of non-toxic phytoplankton (N_i) and zooplankton (Z_i) closely resemble those of toxic phytoplankton (T_i) (see Fig. S1). The parameter values are summarized in Table 1 of the SM.

steady values (see Fig. 4a). When coupling is introduced, the errors decrease over time and converge to substantially smaller steady-state levels. The steady-state synchronization error in the non-coupled system is approximately three to five times larger than that in the coupled system. This indicates that non-synchronized patterns maintain their asynchronous characteristics even after processing synchronization errors (Figs. 5a-c, S3), while synchronized patterns remain coherent under the same treatment (Figs. 5d-f, S3).

The dependence of synchronization error on coupling strength reveals a critical coupling threshold h_c (see Fig. 4b). For $h < h_c$, synchronization remains incomplete, whereas for $h > h_c$ the system consistently converges to a synchronized pattern state. This behavior demonstrates that inter-layer coupling can overcome intrinsic heterogeneities and enforce coherent spatial organization across stratified layers.

2.4. Effects of stochasticity on pattern formation

Natural aquatic environments are subject to persistent environmental fluctuations, motivating an examination of stochastic effects on pattern dynamics. We therefore introduce multiplicative Gaussian white noise into the model and analyze its impact on spatial structures in both non-coupled and coupled regimes.

In the non-coupled system, stochastic perturbations induce markedly different responses across layers. As noise

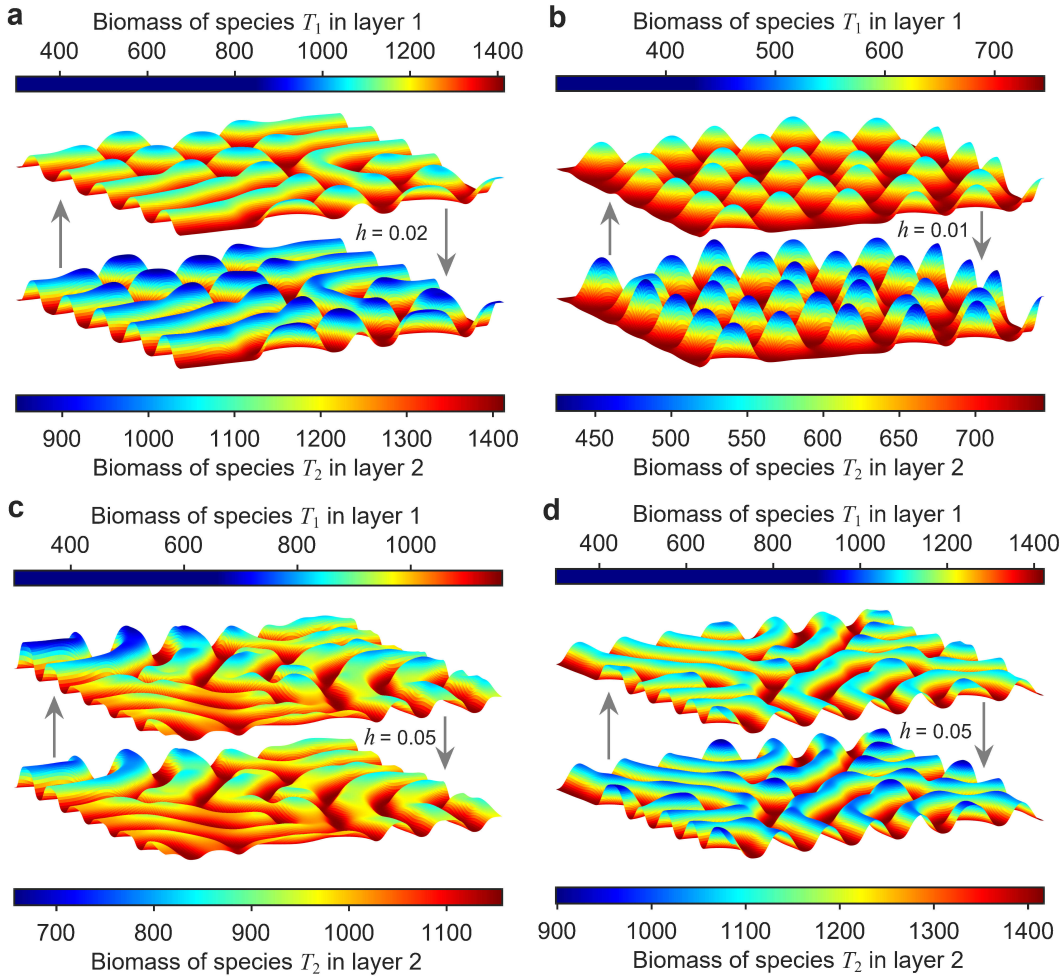


Figure 3: Self-organized synchronization pattern dynamics in the coupled aquatic system with vertical migration. (a-d) With the introduction of coupling, the initially independent spatial patterns from Fig. 2 (e.g., spots, stripes, mixtures) evolve into synchronized states across layers. The merging of the two dispersion-relation peaks at $h = 0$ into a single peak at $h = 0.02$ (see Fig. 1) corresponds to this spatiotemporal synchronization shown in Fig. 3a, and Fig. 3b-d exhibit analogous synchronous behavior. The spatial pattern structures of non-toxic phytoplankton (N_i) and zooplankton (Z_i) closely resemble those of toxic phytoplankton (T_i) (see Fig. S2). The parameter values are summarized in Table 1 of the SM.

intensity increases, the upper layer undergoes a progressive transition from spot-like patterns to stripe-like structures and eventually to pattern collapse, whereas the lower layer retains its spotted configuration over the same range of noise intensities (see Figs. 6a-c, S4). This contrast indicates a layer-dependent sensitivity to stochastic forcing.

When coupling is present, synchronized patterns persist under moderate noise levels and remain qualitatively similar to those observed in deterministic simulations. At sufficiently high noise intensities $\sigma = 0.06$, synchronization degrades and spatial structures become increasingly disordered, with the upper layer again exhibiting more pronounced disruption (see Figs. 6d-f, S4). This asymmetric response indicates that sufficiently strong stochasticity can disrupt the delicate balance maintaining self-organized dynamics, ultimately destroying the coherent spatial structures generated through Turing mechanisms. Our results show that strong stochasticity can destabilize self-organized patterns, even in the presence of coupling, suggesting the crucial role of environmental variability in shaping spatial ecology.

2.5. Robustness of synchronized patterns under stochastic perturbations

Despite the disruptive effects of noise, the coupled system exhibits a pronounced robustness compared to the non-coupled case. While stochasticity leads to substantial asymmetry and degradation of patterns in non-coupled layers, coupling maintains coherent and synchronized spatial structures across layers over a broad range of noise intensities (see Figs. 7, S5).

The impact of noise is also species-dependent. At a noise intensity of $\sigma = 0.05$, the spatial distributions of both phy-

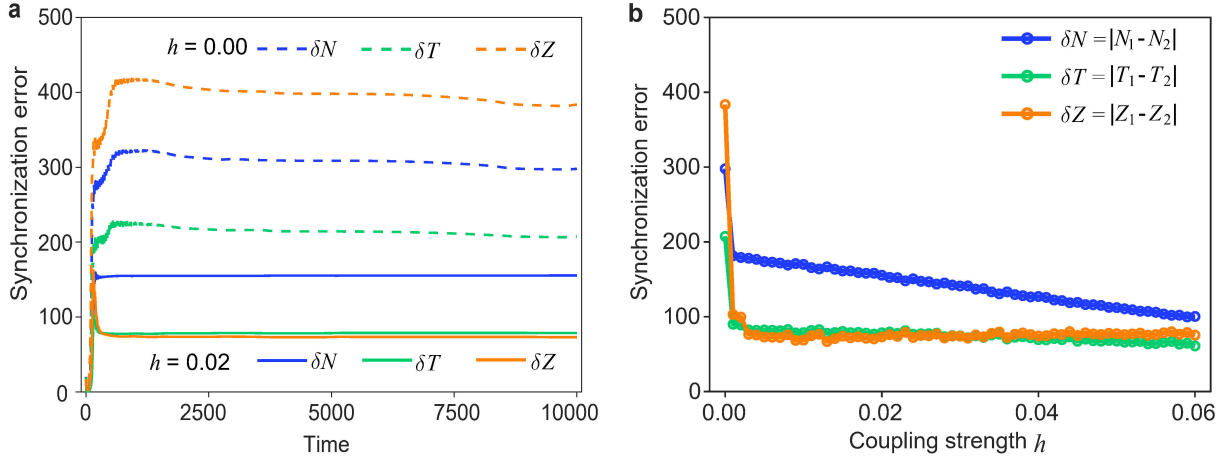


Figure 4: Synchronization error analysis for the coupled aquatic system with vertical migration corresponding to Figs. 2a, 3a. (a) Temporal evolution of the synchronization error for non-coupled ($h = 0$) and coupled ($h = 0.02$) conditions. The error increases and plateaus without coupling, whereas it decreases and plateaus with coupling. The steady-state synchronization error in the non-coupled system is 3 to 5 times larger than that in the coupled system. (b) Steady-state synchronization error as a function of coupling strength h . The error decreases monotonically with increasing h and eventually stabilizes. The parameter values are summarized in Table 1 of the SM.

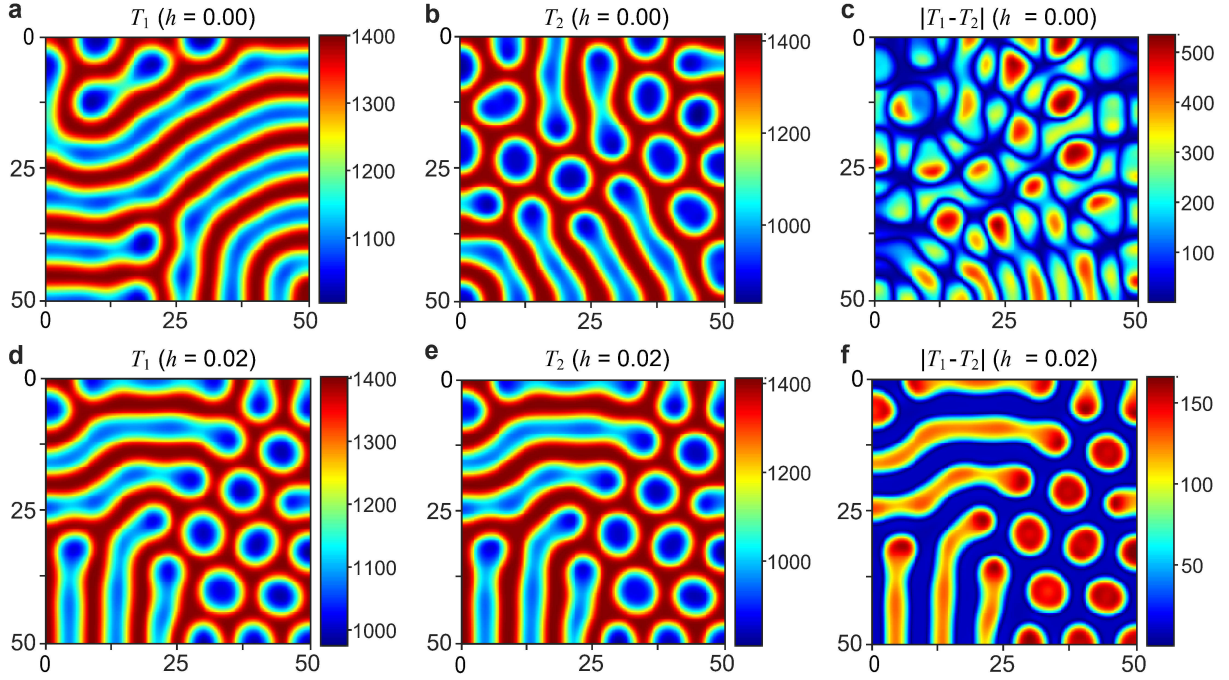


Figure 5: Visual comparison of self-organized patterns and their synchronization errors for non-coupled (Fig. 2a) and coupled (Fig. 3a) systems. (a-c) For the non-coupled system ($h = 0$): (a-b) self-organized patterns, (c) pattern of the synchronization error, which exhibits a structure distinctly different from (a-b). (d-f) For the coupled system ($h = 0.02$): (d-e) synchronized patterns, (f) pattern of the synchronization error, which maintains structural similarity to (d-e). The spatial pattern structures of non-toxic phytoplankton (N_i) and zooplankton (Z_i) closely resemble those of toxic phytoplankton (T_i) (see Fig. S3). The parameter values are summarized in Table 1 of the SM.

toplankton types maintain relatively stable configurations, whereas zooplankton displays pronounced local fluctuations, particularly in the upper layer. Simulations indicate that non-toxic phytoplankton is least affected by stochastic perturbations, toxic phytoplankton shows intermediate sensitivity, and zooplankton exhibits the strongest response, particularly in the upper layer. This hierarchy suggests that higher trophic levels are more susceptible to environmental fluctuations. Importantly, coupling mitigates these layer-specific effects by redistributing disturbances between layers. Zooplankton patterns that fragment under non-coupled conditions recover coherent spatial organization when coupling is introduced. Overall, inter-layer coupling enhances both synchronization and resilience, stabilizing self-organized patterns against

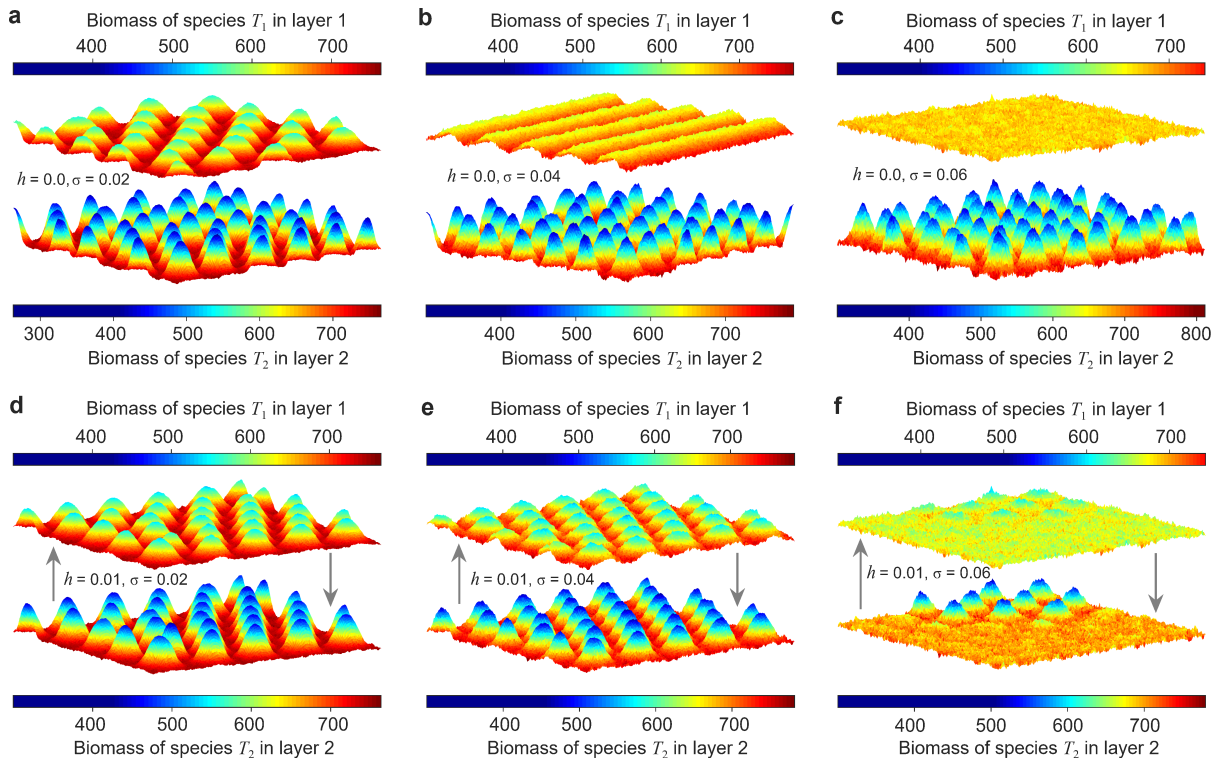


Figure 6: Effect of stochasticity on spotted pattern structures. (a-c) Without coupling, increasing noise intensity affects the upper layer more than the lower layer: the upper-layer pattern transitions from spots to stripes and eventually vanishes, while the lower layer maintains its spotted structure. (d-f) With coupling, the system exhibits robustness to stochastic fluctuations, preserving the spotted structure in both layers until the noise intensity exceeds a critical threshold, beyond which the spatial patterns collapse. The spatial pattern structures of non-toxic phytoplankton (N_i) and zooplankton (Z_i) closely resemble those of toxic phytoplankton (T_i) (see Fig. S4). The parameter values are summarized in Table 1 of the SM.

stochastic perturbations.

3. Discussion

The persistence of coherent spatial patterns in plankton ecosystems, despite pervasive environmental variability, represents a fundamental challenge for understanding self-organization in aquatic systems [6–15, 45]. Although a wide range of biological and physical mechanisms have been proposed to explain plankton patchiness [7, 8, 33], far less attention has been paid to how spatially synchronized patterns remain stable once coupling between domains is established, particularly under stochastic conditions. In this study, we address this issue by demonstrating that gradient coupling between vertically structured plankton layers provides a minimal yet effective mechanism for both synchronization and noise stability.

A central result of our work is the identification of a sharp, coupling-induced transition from layer-specific pattern formation to fully synchronized spatial structures. In the absence of coupling, each layer independently develops Turing-type patterns that are highly susceptible to stochastic perturbations. Once coupling strength exceeds a critical threshold, however, these independent patterns collapse into a unified spatial configuration that remains coherent even under substantial environmental noise. This finding establishes coupling strength as a key control parameter governing the stability and coherence of pattern-forming plankton systems, rather than merely a secondary modifier of pre-existing patterns.

Beyond synchronization, our results reveal that diffusive coupling fundamentally reshapes how environmental noise propagates through the ecosystem. In particular, we uncover a systematic trophic hierarchy in noise sensitivity, with zooplankton populations exhibiting markedly greater vulnerability to stochastic perturbations than phytoplankton. This asymmetry suggests that ecosystem stability under fluctuating conditions is not uniformly distributed across trophic levels but is instead structured by interaction topology and biomass exchange pathways. Such differential sensitivity may contribute to trophic imbalances and may offer mechanistic insight into why higher trophic levels often exhibit earlier or more pronounced responses to environmental variability.

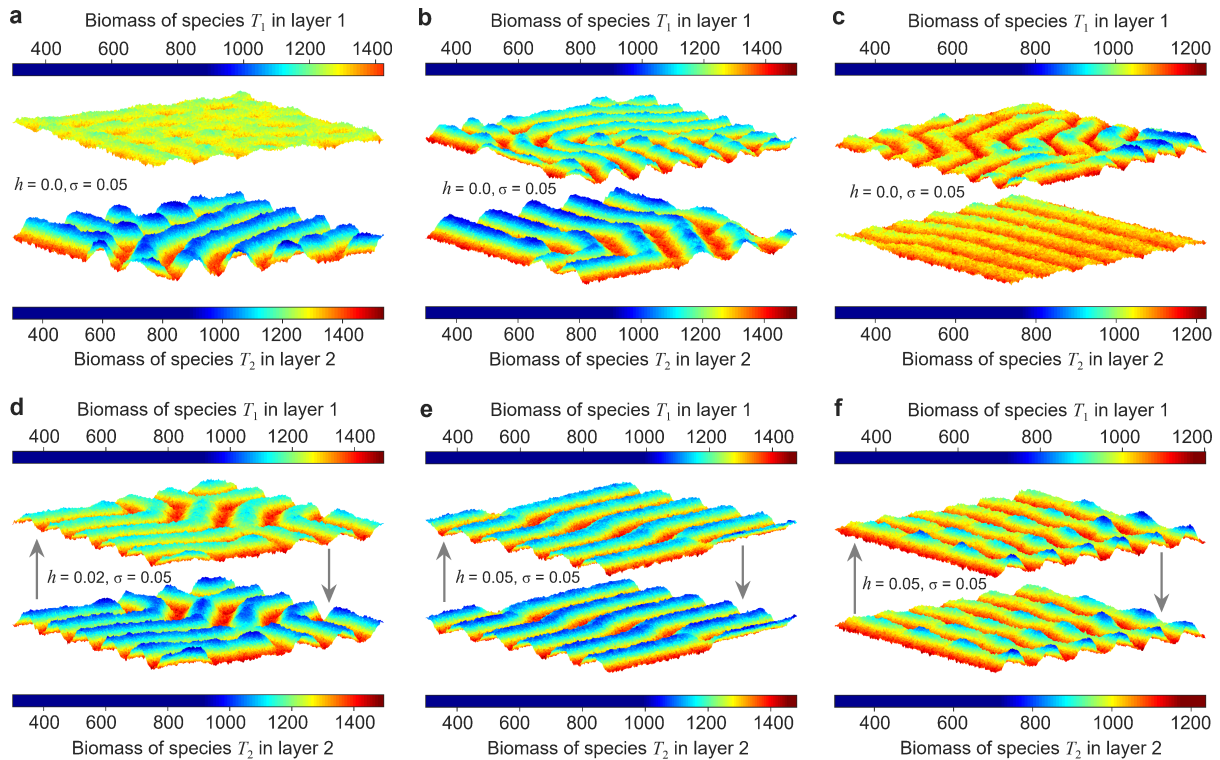


Figure 7: Robust synchronization patterns by coupling in a stochastic environment. (a-c) Without coupling, the two layers maintain distinct and independent spatial patterns in the presence of noise. (d-f) With coupling introduced, the initially different patterns achieve a robust synchronized state, demonstrating that coupling can overcome both initial heterogeneity and stochastic perturbations to establish synchronous dynamics. The spatial pattern structures of non-toxic phytoplankton (N_i) and zooplankton (Z_i) closely resemble those of toxic phytoplankton (T_i) (see Fig. S5). The parameter values are summarized in Table 1 of the SM.

Importantly, the mechanism identified here differs qualitatively from synchronization driven by active biological processes, such as zooplankton vertical migration or adaptive foraging behavior [9, 12, 33, 41, 42]. Whereas these processes rely on species-specific traits and behavioral responses, diffusive coupling is a passive physical mechanism arising from the exchange of individuals or biomass between layers. Our results therefore demonstrate that robust synchronization can emerge even in the absence of complex behavioral regulation, provided that sufficient coupling exists between spatial domains. This distinction clarifies the respective roles of physical coupling and biological adaptation and suggests that some large-scale spatial organization in plankton communities may be explained without invoking finely tuned behavioral strategies.

The ecological significance of synchronization becomes apparent when considering how real stratified ecosystems function. The convergence of upper and lower layers toward coherent spatial patterns does not negate the importance of stratification; rather, it reveals that vertical migration, as exemplified by organisms such as euphausiids (*Euphausia mucronata*) and semi-pelagic squat lobsters (*Pleuroncodes monodon*) in oxygen minimum zones, creates essential functional connectivity across physically distinct habitats [40]. This biological coupling transforms independent dynamical systems into an integrated ecological unit, where synchronized patterns reflect coordinated responses to environmental variability across the water column. Here, stratification provides the fundamental template for niche differentiation, while synchronization ensures system-level coherence. Importantly, synchronization confers measurable benefits that directly address ecosystem stability: global-scale analyses of plankton community interactomes reveal that coordinated dynamics enhance robustness to environmental perturbations, with more tightly connected communities exhibiting lower vulnerability to changing conditions [50]. Our finding that coupled systems exhibit enhanced robustness to stochastic perturbations aligns precisely with this empirical evidence, suggesting that coherent spatial organization actively contributes to ecosystem resilience.

Furthermore, the fact that layers initially support different types of pattern demonstrates that each layer retains its intrinsic self-organizing capacity, reflecting the functional diversity observed in mixotrophic plankton communities, where

flexible foraging strategies allow organisms to occupy distinct ecological niches [51]. Their eventual synchronization under coupling reveals how migratory integration weaves these local dynamics into a coherent whole without erasing underlying heterogeneity. This interplay between local heterogeneity and regional coherence has direct implications for understanding ecosystem functioning: the maintenance of distinct layer-specific dynamics prior to synchronization supports the stoichiometric diversity observed across trophic levels, which underpins energy transfer efficiency and population persistence under environmental stress [52]. Thus, stratification provides the necessary spatial structure for functional specialization, while biologically mediated synchronization ensures that these specialized components operate in concert, buffering the system against localized disturbances, and promoting long-term stability.

From a theoretical perspective, our findings place the classical Turing instability in a broader ecological context. Rather than acting as a global system-wide property, pattern-forming instabilities operate locally within layers, while inter-layer coupling determines whether these patterns remain fragmented or become synchronized across space. Environmental noise further modulates this balance, selectively destabilizing non-coupled configurations while leaving coupled systems comparatively robust. This interplay between local instability, coupling, and stochasticity offers a unifying framework for understanding why coherent plankton patterns are frequently observed in noisy aquatic environments.

The framework presented here is intentionally minimal and does not explicitly incorporate adaptive behaviors, species diversity beyond a simple trophic structure, or complex hydrodynamic forcing. In natural ecosystems, these factors are likely to interact with diffusive coupling in nontrivial ways. Future work should therefore explore how passive coupling interacts with active migration, adaptive foraging, and higher trophic complexity, as well as how the noise robustness identified here extends to more diverse food webs [53–55]. Nonetheless, by isolating diffusive coupling as a core organizing mechanism, our results provide a parsimonious baseline for interpreting the emergence and persistence of coherent spatial patterns in fluctuating aquatic ecosystems.

4. Methods

We investigated the spatiotemporal dynamics of a spatially explicit, two-layer aquatic ecosystem model describing interactions among non-toxic phytoplankton (N_i), toxic phytoplankton (T_i), and zooplankton (Z_i) distributed across two vertically stratified water layers ($i = 1, 2$). The system is formulated as a set of coupled reaction-diffusion equations incorporating species-specific diffusion, biologically motivated cross-diffusion, and inter-layer exchange representing vertical migration.

4.1. Numerical simulations

Computational domain and discretization. All simulations were conducted on a two-dimensional square domain of size 50×50 , representing a horizontally extended aquatic habitat. The domain was discretized using a uniform Cartesian grid with spatial steps $\delta x = \delta y = 0.25$, yielding a total of 201×201 grid points. This spatial resolution was sufficient to resolve the characteristic wavelengths of the emerging Turing patterns observed in the system.

Time integration. Temporal evolution was computed using an explicit forward Euler scheme with a fixed time step $\delta t = 0.01$. This choice ensures numerical stability and adequate temporal resolution for the reaction-diffusion dynamics under the parameter regimes considered. Each simulation was run for 10,000 time steps, allowing transient behavior to decay and long-term spatiotemporal patterns to fully develop.

Boundary conditions. Zero-flux (von Neumann) boundary conditions were imposed on all state variables at the domain boundaries, ensuring that no population flux occurs across the system edges. These conditions correspond to an isolated ecosystem and conserve total biomass within the computational domain.

Stochastic framework. To account for environmental variability, stochastic perturbations were incorporated in the form of multiplicative Gaussian white noise applied to all population variables. At each time step, noise terms with intensity σ were added and scaled by $\sqrt{\delta t}$ to ensure appropriate temporal scaling. The stochastic simulations were implemented using a Monte Carlo approach. To maintain biological realism and numerical stability, population densities were constrained to remain non-negative throughout the simulations.

Initial conditions. Simulations were initialized with spatially heterogeneous population distributions to reflect natural patchiness in aquatic ecosystems and to allow spontaneous symmetry breaking. Initial biomasses were set as spatially uniform backgrounds with superimposed random perturbations: $N_i(0) = 500 \pm 100$, $T_i(0) = 300 \pm 50$, and $Z_i(0) =$

100 ± 20 across the domain. These initial conditions do not impose any predefined spatial structure and serve solely to trigger pattern-forming instabilities.

4.2. Model processes

Biological Interactions. The model incorporates several key ecological processes: (1) logistic population growth with inter-specific competition between phytoplankton types, (2) type-II functional response for zooplankton grazing, (3) biomass conversion with distinct efficiencies for toxic and non-toxic prey, (4) density-dependent mortality, and (5) vertical migration between water layers.

Spatial processes. Population dispersal within each layer is described by standard diffusion terms with species-specific diffusion coefficients. In addition, cross-diffusion terms are included to model directed zooplankton movement in response to phytoplankton gradients, capturing avoidance of toxic phytoplankton and attraction toward non-toxic prey. These terms provide a mechanistic representation of behaviorally mediated movement and play a critical role in the emergence of spatial patterns.

Acknowledgments

We thank Tousheng Huang for helpful discussions. This study was funded by the National Natural Science Foundation of China (32525006, 32330064), and the Fundamental and Interdisciplinary Disciplines Breakthrough Plan of the Ministry of Education of China (JYB2025XDXM902).

Conflict of interest

The authors declare that they have no known competing financial interests or personal relationships that could have appeared to influence the work reported in this paper.

Author contributions

J.K. and C.C conceived the project and planned the study. All authors supervised the study, developed the model, analyzed the data, carried out the theoretical analysis and numerical simulations, analyzed the simulation results, and wrote the paper.

Data and code availability

No data was used for the research described in this paper.

References

- [1] Natalie L. Geyer, Markus Huettel, Michael S. Wetz. (2018) Phytoplankton Spatial Variability in the River-Dominated Estuary, Apalachicola Bay, Florida. [Estuaries and Coasts 41: 2024-2038.](#)
- [2] Simon van Gennip, Adrian P. Martin, Meric A. Srokosz, John T. Allen, Rosalind Pidcock, Stuart C. Painter, Mark C. Stinchcombe. (2016) Plankton patchiness investigated using simultaneous nitrate and chlorophyll observations. [Journal of Geophysical Research: Oceans 121\(6\): 4149-4156.](#)
- [3] Matias Scheinin, Matias Scheinin, Eero Asmala, Eero Asmala. (2020) Ubiquitous Patchiness in Chlorophyll a Concentration in Coastal Archipelago of Baltic Sea. [Frontiers in Marine Science 7: 563.](#)
- [4] Kelly L. Robinson, Su Sponaugle, Jessica Y. Luo, Miram R. Gleiber, Robert K. Cowen. (2021) Big or small, patchy all: Resolution of marine plankton patch structure at micro- to submesoscales for 36 taxa. [Science Advances 7: eabk2904.](#)
- [5] Johan van de Koppel, Max Rietkerk, Norbert Dankers, Peter M.J. Herman. (2005) Scale-dependent feedback and regular spatial patterns in young mussel beds. [The American Naturalist 165\(3\): E66-77.](#)
- [6] Feifan Zhang, Jiamin Sun, Wang Tian. (2022) Spatiotemporal pattern selection in a nontoxic-phytoplankton - toxic-phytoplankton - zooplankton model with toxin avoidance effects. [Applied Mathematics and Computation 423: 127007.](#)
- [7] Tousheng Huang, Chengfeng Yu , Zequn Lin , Huayong Zhang , Rui Liu , Ruyin Li , Yifan Yang , Yonglan Tian.

- (2024) Self-organization of nested patterns in a coupled spatiotemporal phytoplankton-zooplankton system. [Communications in Nonlinear Science and Numerical Simulation 130: 107804](#).
- [8] Tousheng Huang, Chengfeng Yu, Kui Zhang, Xingyu Liu, Jiulong Zhen, Lan Wang. (2023) Complex pattern dynamics and synchronization in a coupled spatiotemporal plankton system with zooplankton vertical migration. [Chaos, Solitons and Fractals 175: 114063](#).
- [9] Carol L. Folt, Carolyn W. Burns. (1999) Biological drivers of zooplankton patchiness. [Trends in Ecology & Evolution 14\(8\): 300-305](#).
- [10] Levin SA, Segel LA. (1976) Hypothesis for origin of planktonic patchiness. [Nature 259: 659](#).
- [11] Alexander B. Medvinsky, Sergei V. Petrovskii, Irene A. Tikhonova, Horst Malchow, Bai-Lian Li. (2002) Spatiotemporal complexity of plankton and fish dynamics. [SIAM Review 44\(3\): 311-370](#).
- [12] Jennifer C. Prairie, Kelly R. Sutherland, Kerry J. Nickols, Amanda M. Kaltenberg. (2012) Biophysical interactions in the plankton: A cross-scale review. [Limnology and Oceanography: Fluids and Environments 2\(1\): 121-145](#).
- [13] Edward R. Abraham. (1998) The generation of plankton patchiness by turbulent stirring. [Nature 391: 577-580](#).
- [14] William M. Durham, Eric Climent, Michael Barry, Filippo De Lillo, Guido Boffetta, Massimo Cencini, Roman Stocker. (2013) Turbulence drives microscale patches of motile phytoplankton. [Nature Communications 4: 2148](#).
- [15] A.P. Martin. (2003) Phytoplankton patchiness: the role of lateral stirring and mixing. [Progress in Oceanography 57\(2\): 125-174](#).
- [16] David Karig, K. Michael Martini, Ting Lu, Nicholas A. DeLateur, Nigel Goldenfeld, Ron Weiss. (2018) Stochastic Turing patterns in a synthetic bacterial population. [PNAS 115\(26\): 6572-6577](#).
- [17] Francesca Di Patti, Yamel Ugartechea Chirino, Rinat Arbel-Goren, Tom Sharon, Aaron Castillo, Elena Alvarez-Buylla, Duccio Fanelli, Joel Stavans. (2023) Stochastic Turing patterns of trichomes in Arabidopsis leaves. [PNAS 120\(42\): e2309616120](#).
- [18] Turriff N, Runge, JA, Cembella AD. (1995) Toxin accumulation and feeding behaviour of the planktonic copepod *Calanus finmarchicus* exposed to the red-tide dinoflagellate *Alexandrium excavatum*. [Marine Biology 123: 55-64](#).
- [19] Mette Schultz, Thomas Kiørboe. (2009) Active prey selection in two pelagic copepods feeding on potentially toxic and non-toxic dinoflagellates. [Journal of Plankton Research 31\(5\): 553-561](#).
- [20] Joydeep Pal, S. Bhattacharya, J. Chattopadhyay. (2010) Does predator go for size selection or preferential toxic-nontoxic species under limited resource? [OnLine Journal of Biological Sciences 10\(1\): 11-16](#).
- [21] Gregory J. Teegarden. (1999) Copepod grazing selection and particle discrimination on the basis of PSP toxin content. [Marine Ecology Progress Series 181: 163-176](#).
- [22] Peter L. Starkweather, Penelope E. Kellar. (1983) Utilization of cyanobacteria by *Brachionus calyciflorus*: *Anabaena flos-aquae* (NRC-44-1) as a sole or complementary food source. [Hydrobiologia 104: 373-377](#).
- [23] Takayuki Hanazato, Masayuki Yasuno. (1987) Experimental studies on competition between *Bosmina longirostris* and *Bosmina fatalis*. [Hydrobiologia 154: 189-199](#).
- [24] Rolland S. Fulton. (1988) Resistance to blue-green algal toxins by *Bosmina longirostris*. [Journal of Plankton Research 10\(4\): 771-778](#).
- [25] William R. DeMott, Qing-Xue Zhang, Wayne W. Carmichael. (1991) Effects of toxic cyanobacteria and purified toxins on the survival and feeding of a copepod and three species of *Daphnia*. [Limnology and Oceanography 36\(7\): 1346-1357](#).
- [26] Rainer Kurmayer, Friedrich Jüttner. (1999) Strategies for the co-existence of zooplankton with the toxic cyanobacterium *Planktothrix rubescens* in Lake Zurich. [Journal of Plankton Research 21\(4\): 659-683](#).
- [27] Albert Calbet, Dolors Vaqué, Jordi Felipe, Magda Vila, Maria Montserrat Sala, Miquel Alcaraz, Marta Estrada. (2003) Relative grazing impact of microzooplankton and mesozooplankton on a bloom of the toxic dinoflagellate *Alexandrium minutum*. [Marine Ecology Progress Series 259: 303-309](#).
- [28] LE Schmidt, Per Juel Hansen. (2001) Allelopathy in the Prymnesiophyte *Chrysochromulina polylepis*: Effect of Cell Concentration, Growth Phase and pH. [Marine Ecology Progress Series 216: 67-81](#).
- [29] Allan Cembella. (2003) Chemical ecology of eukaryotic microalgae in marine ecosystems. [Phycologia 42\(4\): 420-447](#).
- [30] Gordon V. Wolfe. (2000) The Chemical Defense Ecology of Marine Unicellular Plankton: Constraints, Mechanisms,

- and Impacts. [Biological Bulletin 198\(2\): 225-44.](#)
- [31] V.V. Sukhanov, A.M. Omelko. (2002) Dynamics of feeding preferences by a predator. [Ecological Modelling 154\(3\): 203-206.](#)
- [32] Jordi Solé, Emilio García-Ladona, Marta Estrada. (2006) The role of selective predation in harmful algal blooms. [Journal of Marine Systems 62\(1\): 46-54.](#)
- [33] Bingzhang Chen, Eiji Masunaga, Sherwood Lan Smith, Hidekatsu Yamazaki. (2020) Diel vertical migration promotes zooplankton horizontal patchiness. [Journal of Oceanography 77\(1\): 123-135.](#)
- [34] Kanchana Bandara, Øystein Varpe, Lishani Wijewardene, Vigdis Tverberg, Ketil Eiane. (2021) Two hundred years of zooplankton vertical migration research. [Biological Reviews 96\(4\): 1547-1589.](#)
- [35] Shane A. Richards, Hugh P. Possingham, John Noye. (1996) Diel vertical migration: modelling light-mediated mechanisms. [Journal of Plankton Research 18\(14\): 2199-2222.](#)
- [36] Maciej Z. Gliwicz. (1986) Predation and the evolution of vertical migration in zooplankton. [Nature 320: 746-748.](#)
- [37] Stefano Simoncelli, Stephen J. Thackeray, Danielle J. Wain. (2019) Effect of temperature on zooplankton vertical migration velocity. [Hydrobiologia 829: 143-166.](#)
- [38] Monica Winder, Boersma M, Spaak P. (2003) On the cost of vertical migration: Are feeding conditions really worse at greater depths? [Freshwater Biology 48\(3\): 383-393.](#)
- [39] Xabier Irigoien, David V. P. Conway, Roger P. Harris. (2004) Flexible diel vertical migration behaviour of zooplankton in the Irish Sea. [Marine Ecology Progress Series 267: 85-97.](#)
- [40] Rainer Kiko, Helena Hauss. (2019) On the Estimation of Zooplankton-Mediated Active Fluxes in Oxygen Minimum Zone Regions. [Frontiers in Marine Science 6:741.](#)
- [41] Kendra L. Daly, Walker O. Smith Jr. (1993) Physical-Biological Interactions Influencing Marine Plankton Production. [Annual Review of Ecology and Systematics 24\(1\): 555-585.](#)
- [42] Andrew Yu. Morozov, Sergei V. Petrovskii, Nikolay P. Nezlin. (2007) Towards resolving the paradox of enrichment: The impact of zooplankton vertical migrations on plankton systems stability. [Journal of Theoretical Biology 248\(3\): 501-511.](#)
- [43] Kalevi Salonen, Marko Järvinen, Taavi Aalto, Markit Likolammi, Visa Lindblom, Uwe Münster, Jouko Sarvala. (2024) Dynamic adaptation of phytoplankton vertical migration to changing grazing and nutrient conditions. [Hydrobiologia 851: 3639-3663.](#)
- [44] Yonghong Chen, Govindan Rangarajan, Mingzhou Ding. (2006) Stability of synchronized dynamics and pattern formation in coupled systems: Review of some recent results. [Communications in Nonlinear Science and Numerical Simulation 11\(8\): 934-960.](#)
- [45] Subhendu Chakraborty, Sabyasachi Bhattacharya, Ulrike Feudel, J. Chattopadhyay. (2012) The role of avoidance by zooplankton for survival and dominance of toxic phytoplankton. [Ecological Complexity 11: 144-153.](#)
- [46] A.M. Turing. (1952) The Chemical Basis of Morphogenesis. [Philosophical Transactions of the Royal Society of London. Series B, Biological Sciences 237\(641\): 37-72.](#)
- [47] J.D. Murray. *Mathematical Biology III: Spatial Models and Biomedical Applications.* Springer New York, NY.
- [48] Xiao-Chong Zhang, Gui-Quan Sun, and Zhen Jin. (2012) Spatial dynamics in a predator-prey model with Beddington-DeAngelis functional response. [Physical Review E 85\(2\): 021924.](#)
- [49] Lin Xue. (2012) Pattern formation in a predator-prey model with spatial effect. [Physica A 351\(2\): 021924.](#)
- [50] Samuel Chaffron et al. (2021) Environmental vulnerability of the global ocean epipelagic plankton community interactome. [Science. Advances 7: eabg1921.](#)
- [51] Ben A. Ward. (2019) Mixotroph ecology: More than the sum of its parts. [PNAS 116\(13\): 5846-5848.](#)
- [52] Mingjun Feng, Haowu Cheng, Peiyu Zhang, Kang Wang, Tao Wang, Huan Zhang, Huan Wang, Libin Zhou, Jun Xu, Min Zhang. (2023) Stoichiometric stability of aquatic organisms increases with trophic level under warming and eutrophication. [Science of The Total Environment 858: 160106.](#)
- [53] Ju Kang, Shijie Zhang, Yiyuan Niu, Fan Zhong, Xin Wang. (2024) Intraspecific predator interference promotes biodiversity in ecosystems. [eLife 13: RP93115.](#)
- [54] Ju Kang, Shijie Zhang, Yiyuan Niu, Fan Zhong, Xin Wang. (2024) Self-organized biodiversity in biotic resource systems through pairwise encounters. [Chaos, Solitons and Fractals 188: 115607.](#)

- [55] Ju Kang, Yiyuan Niu, Yuanzhi Li, Chengjin Chu. (2026) Self-organized biodiversity and species abundance distribution patterns in ecosystems with higher-order interactions. [Chaos, Solitons and Fractals 202: 117442.](#)

Supplementary Materials

I. Turing bifurcation analysis of the coupled system

In this work, we investigate the reaction-diffusion systems in coupled spatiotemporal aquatic ecosystems characterized by vertical migration as follows:

$$\begin{cases} \frac{\partial N_1(x,y,t)}{\partial t} = r_{11}N_1 \left(1 - \frac{N_1 + \alpha_{11}T_1}{K_{11}}\right) - \frac{w_{11}N_1Z_1}{p_{11} + N_1} + d_{11}\Delta N_1 + h_{11}(N_2 - N_1), (x,y) \in \Omega, t > 0, \\ \frac{\partial T_1(x,y,t)}{\partial t} = r_{12}T_1 \left(1 - \frac{T_1 + \alpha_{12}N_1}{K_{12}}\right) - \frac{w_{12}T_1Z_1}{p_{12} + T_1 + \beta_1N_1} + d_{12}\Delta T_1 + h_{12}(T_2 - T_1), (x,y) \in \Omega, t > 0, \\ \frac{\partial Z_1(x,y,t)}{\partial t} = \frac{c_{11}w_{11}N_1Z_1}{p_{11} + N_1} - \frac{c_{12}w_{12}T_1Z_1}{p_{12} + T_1 + \beta_1N_1} - m_1Z_1 + d_{13}\Delta Z_1 + d_{31}Z_1\Delta N_1 - d_{32}Z_1\Delta T_1 + h_{13}(Z_2 - Z_1), (x,y) \in \Omega, t > 0, \\ \frac{\partial N_2(x,y,t)}{\partial t} = r_{21}N_2 \left(1 - \frac{N_2 + \alpha_{21}T_2}{K_{21}}\right) - \frac{w_{21}N_2Z_2}{p_{21} + N_2} + d_{21}\Delta N_2 + h_{21}(N_1 - N_2), (x,y) \in \Omega, t > 0, \\ \frac{\partial T_2(x,y,t)}{\partial t} = r_{22}T_2 \left(1 - \frac{T_2 + \alpha_{22}N_2}{K_{22}}\right) - \frac{w_{22}T_2Z_2}{p_{22} + T_2 + \beta_2N_2} + d_{22}\Delta T_2 + h_{22}(T_1 - T_2), (x,y) \in \Omega, t > 0, \\ \frac{\partial Z_2(x,y,t)}{\partial t} = \frac{c_{21}w_{21}N_2Z_2}{p_{21} + N_2} - \frac{c_{22}w_{22}T_2Z_2}{p_{22} + T_2 + \beta_2N_2} - m_2Z_2 + d_{23}\Delta Z_2 + d_{41}Z_2\Delta N_2 - d_{42}Z_2\Delta T_2 + h_{23}(Z_1 - Z_2), (x,y) \in \Omega, t > 0, \\ \frac{\partial N_i(x,y,t)}{\partial n} = \frac{\partial T_i(x,y,t)}{\partial n} = \frac{\partial Z_i(x,y,t)}{\partial n} = 0, i = 1, 2, (x,y) \in \partial\Omega, t > 0, \\ N_i(x,y,t) > 0, T_i(x,y,t) > 0, Z_i(x,y,t) > 0, (x,y) \in \Omega. \end{cases} \quad (S1)$$

Here, from the ecological perspective, our focus is on the coexistence state $E^*=(N_1^*, T_1^*, Z_1^*, N_2^*, T_2^*, Z_2^*)$ of the system (S1) in both layers. As established, vertical environmental heterogeneity is modeled through inter-layer parameter variations. Theoretically, the impact of varying any parameter subset on the pattern formation in system (S1) can be investigated.

In addition, the non-spatial coexistence steady state (N_1^*, T_1^*, Z_1^*) of a non-coupled single system is well-established in previous research [6, 45]. Hence, we are interested in studying the stability of the coexisting equilibrium E^* within coupled system (S1). Hence, the Jacobian matrix of the non-spatial form of system (S1) associated with $E^*=(N_1^*, T_1^*, Z_1^*, N_2^*, T_2^*, Z_2^*)$ can be obtained as follows

$$J = \begin{pmatrix} a_{11} & a_{12} & a_{13} & a_{14} & 0 & 0 \\ a_{21} & a_{22} & a_{23} & 0 & a_{25} & 0 \\ a_{31} & a_{32} & a_{33} & 0 & 0 & a_{36} \\ a_{41} & 0 & 0 & a_{44} & a_{45} & a_{46} \\ 0 & a_{52} & 0 & a_{54} & a_{55} & a_{56} \\ 0 & 0 & a_{63} & a_{64} & a_{65} & a_{66} \end{pmatrix}, \quad (S2)$$

where $a_{11} = -h_{11} - \frac{p_{11}w_{11}Z_1^*}{(N_1^* + p_{11})^2} + \frac{r_{11}(K_{11} - 2N_1^* - T_1^*\alpha_{11})}{K_{11}}$, $a_{12} = -\frac{N_1^*r_{11}\alpha_{11}}{K_{11}}$, $a_{13} = -\frac{N_1^*w_{11}}{N_1^* + p_{11}}$, $a_{14} = h_{11}$, $a_{21} = -\frac{r_{12}T_1^*\alpha_{12}}{K_{12}} + \frac{T_1^*w_{12}Z_1^*\beta_1}{(p_{12} + T_1^* + N_1^*\beta_1)^2}$, $a_{22} = -h_{12} + \frac{r_{12}(K_{12} - 2T_1^* - N_1^*\alpha_{12})}{K_{12}} - \frac{w_{12}Z_1^*(p_{12} + N_1^*\beta_1)}{(p_{12} + T_1^* + N_1^*\beta_1)^2}$, $a_{23} = -\frac{T_1^*w_{12}}{p_{12} + T_1^* + N_1^*\beta_1}$, $a_{25} = h_{12}$, $a_{31} = \frac{Z_1^*c_{11}p_{11}w_{11}}{(N_1^* + p_{11})^2} + \frac{Z_1^*c_{12}T_1^*w_{12}\beta_1}{(p_{12} + T_1^* + N_1^*\beta_1)^2}$, $a_{32} = -\frac{c_{12}w_{12}Z_1^*(p_{12} + N_1^*\beta_1)}{(p_{12} + T_1^* + N_1^*\beta_1)^2}$, $a_{33} = -h_{13} - m_1 + \frac{c_{11}N_1^*w_{11}}{N_1^* + p_{11}} - \frac{c_{12}T_1^*w_{12}}{p_{12} + T_1^* + N_1^*\beta_1}$, $a_{36} = h_{13}$, $a_{41} = h_{21}$, $a_{44} = -h_{21} - \frac{p_{21}w_{21}Z_2^*}{(N_2^* + p_{21})^2} + \frac{r_{21}(K_{21} - 2N_2^* - T_2^*\alpha_{21})}{K_{21}}$, $a_{45} = -\frac{N_2^*r_{21}\alpha_{21}}{K_{21}}$, $a_{46} = -\frac{N_2^*w_{21}}{N_2^* + p_{21}}$, $a_{52} = h_{22}$, $a_{54} = -\frac{r_{22}T_2^*\alpha_{22}}{K_{22}} + \frac{T_2^*w_{22}Z_2^*\beta_2}{(p_{22} + T_2^* + N_2^*\beta_2)^2}$, $a_{55} = -h_{22} + \frac{r_{22}(K_{22} - 2T_2^* - N_2^*\alpha_{22})}{K_{22}} - \frac{w_{22}Z_2^*(p_{22} + N_2^*\beta_2)}{(p_{22} + T_2^* + N_2^*\beta_2)^2}$, $a_{56} = -\frac{T_2^*w_{22}}{p_{22} + T_2^* + N_2^*\beta_2}$, $a_{63} = h_{23}$, $a_{64} = \frac{Z_2^*c_{21}p_{21}w_{21}}{(N_2^* + p_{21})^2} + \frac{Z_2^*c_{22}T_2^*w_{22}\beta_2}{(p_{22} + T_2^* + N_2^*\beta_2)^2}$, $a_{65} = -\frac{c_{22}w_{22}Z_2^*(p_{22} + N_2^*\beta_2)}{(p_{22} + T_2^* + N_2^*\beta_2)^2}$, $a_{66} = -h_{23} - m_2 + \frac{c_{21}N_2^*w_{21}}{N_2^* + p_{21}} - \frac{c_{22}T_2^*w_{22}}{p_{22} + T_2^* + N_2^*\beta_2}$.

Following the theoretical analysis of Turing bifurcation in reaction-diffusion systems [6, 7, 48, 49], we introduced small perturbations to the heterogeneous steady state

$$\begin{pmatrix} N_1 \\ T_1 \\ Z_1 \\ N_2 \\ T_2 \\ Z_2 \end{pmatrix} = \begin{pmatrix} N_1^* \\ T_1^* \\ Z_1^* \\ N_2^* \\ T_2^* \\ Z_2^* \end{pmatrix} + \varepsilon \begin{pmatrix} N_{1k} \\ T_{1k} \\ Z_{1k} \\ N_{2k} \\ T_{2k} \\ Z_{2k} \end{pmatrix} e^{\lambda t + i\mathbf{k}\cdot\boldsymbol{\rho}} + c.c. + O(\varepsilon^2), \quad (S3)$$

where $N_{1k}, T_{1k}, Z_{1k}, N_{2k}, T_{2k}$, and Z_{2k} are the perturbations corresponding to N_1, T_1, Z_1, N_2, T_2 and Z_2 , respectively;

$\boldsymbol{\rho} = (x, y)$ is the spatial vector in two dimensional space; λ stands for the growth rate of heterogeneous perturbations in time; i represents the imaginary unit and $i^2 = -1$; \mathbf{k} is the corresponding vector of wavenumbers and $\mathbf{k} \cdot \mathbf{k} = k^2$; c.c. represents complex conjugate. The uniform steady state's linear instability ($\varepsilon \ll 1$) is derived from the dispersion relations. The characteristic equation for $\lambda_1, \lambda_2, \dots, \lambda_6$ can be calculated from $\det(J_k) = 0$, where

$$J_k = J - J_D k^2, \quad (\text{S4})$$

in which

$$J_D = \begin{pmatrix} d_{11} & 0 & 0 & 0 & 0 & 0 \\ 0 & d_{12} & 0 & 0 & 0 & 0 \\ -d_{31}Z_1^* & d_{32}Z_1^* & d_{13} & 0 & 0 & 0 \\ 0 & 0 & 0 & d_{21} & 0 & 0 \\ 0 & 0 & 0 & 0 & d_{22} & 0 \\ 0 & 0 & 0 & -d_{41}Z_2^* & d_{42}Z_2^* & d_{23} \end{pmatrix}, \quad (\text{S5})$$

From $\det(J_k) = 0$, we get the eigenvalues as the roots of the following equation:

$$\lambda^6 + b_5(k^2)\lambda^5 + b_4(k^2)\lambda^4 + b_3(k^2)\lambda^3 + b_2(k^2)\lambda^2 + b_1(k^2)\lambda + b_0(k^2) = 0, \quad (\text{S6})$$

Based on the theory of Turing pattern formation, the sixth-order characteristic Eq. S6 can be addressed through numerical computation to determine the eigenvalues λ_k . We choose d_{31} as the control parameter for bifurcation analysis. According to the principles of Turing instability, the emergence of Turing patterns is initiated when

$$\text{Re}(\lambda_k) = 0, \text{Im}(\lambda_k) = 0 \text{ at } k = k_T \neq 0. \quad (\text{S7})$$

Condition (S7) is satisfied only if the constant term of Eq. (S6) equals zero, i.e., $b_0(k^2) = 0$.

II. Supplemental Tables

Table 1: Parameter values used in the simulations of Figs. 1-7.

Figure	Layer	Parameter values																				
		r_{i1}	r_{i2}	α_{i1}	α_{i2}	K_{i1}	K_{i2}	c_{i1}	c_{i2}	w_{i1}	w_{i2}	p_{i1}	p_{i2}	β_i	m_i	d_{i1}	d_{i2}	d_{i3}	d_{3i}	d_{4i}	h_{il}	σ
Figs. 1, 2a, 3a, 4, 5, 7a, 7d	1	0.56	0.49	0.25	0.1	1600	1500	0.45	0.4	0.45	0.4	150	140	2	0.1	1	0.1	0.001	0.0006	0.0005	[0,0.06]	[0,0.06]
	2	0.56	0.49	0.25	0.1	1600	1500	0.45	0.4	0.45	0.4	150	140	2	0.1	1	0.1	0.001	0.0012	0.0007	[0,0.06]	[0,0.06]
Figs. 2b, 3b, 6	1	0.56	0.49	0.25	0.1	800	800	0.45	0.4	0.45	0.4	150	140	2	0.1	1	0.1	0.001	0.0015	0.001	[0,0.06]	[0,0.06]
	2	0.56	0.49	0.25	0.1	800	800	0.45	0.4	0.45	0.4	150	140	2	0.1	1	0.1	0.001	0.0009	0.0003	[0,0.06]	[0,0.06]
Figs. 2c, 3c, 7b, 7e	1	0.56	0.49	0.25	0.1	1500	1500	0.45	0.4	0.5	0.5	80	70	2	0.1	1	0.1	0.001	0.0004	0.0002	[0,0.06]	[0,0.06]
	2	0.56	0.49	0.25	0.1	1500	1500	0.45	0.4	0.5	0.5	80	70	2	0.1	1	0.1	0.001	0.0012	0.0008	[0,0.06]	[0,0.06]
Figs. 2d, 3d, 7c, 7f	1	0.66	0.62	0.25	0.1	1200	1200	0.45	0.4	0.5	0.5	50	30	2	0.1	1	0.1	0.001	0.001	0.0005	[0,0.06]	[0,0.06]
	2	0.56	0.59	0.25	0.1	1200	1200	0.45	0.4	0.5	0.5	50	30	2	0.1	1	0.1	0.001	0.0012	0.0008	[0,0.06]	[0,0.06]

III. Supplemental Figures

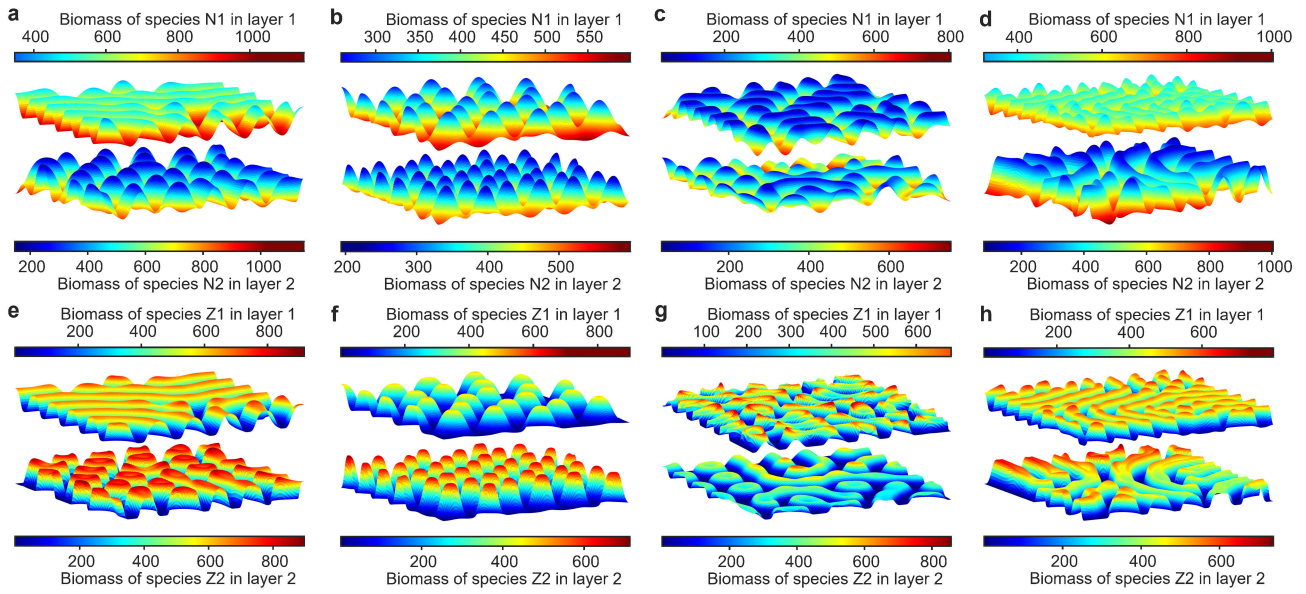


Figure S1: Self-organized pattern dynamics in the non-coupled aquatic system (without vertical migration). (a-h) Spatial patterns in the surface (Layer 1) and bottom (Layer 2) layers exhibit distinct structural forms, such as spots, stripes, and mixtures. The parameter values are the same as Fig. 2.

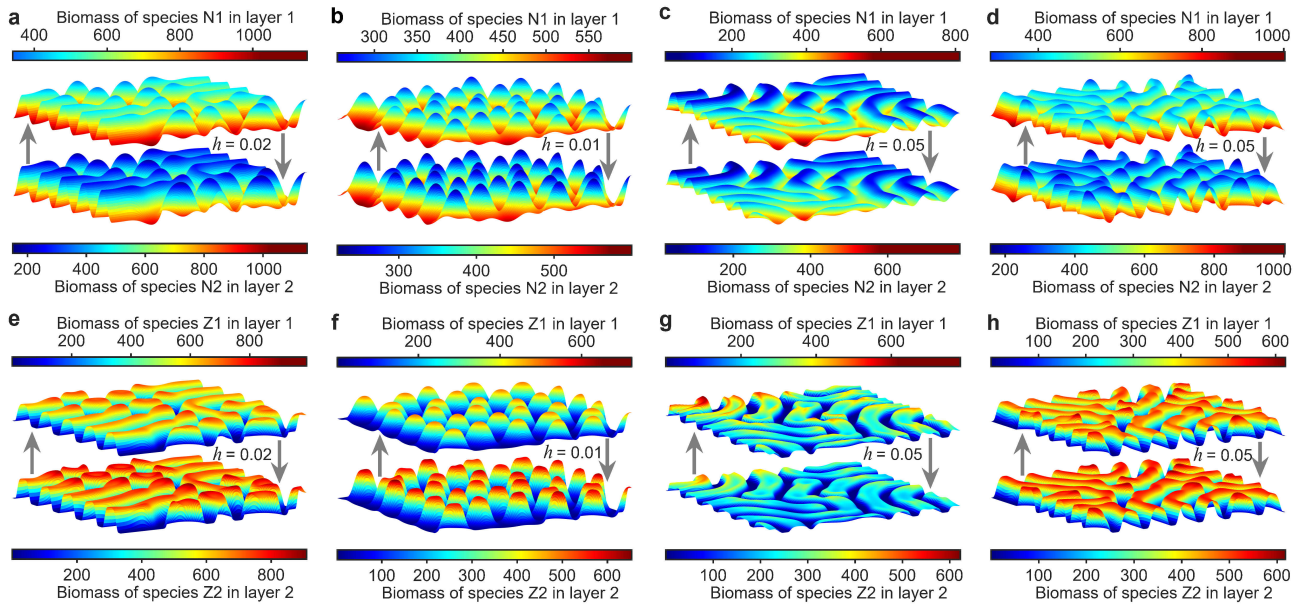


Figure S2: Self-organized synchronization pattern dynamics in the coupled aquatic system with vertical migration. (a-h) With the introduction of coupling, the initially independent spatial patterns from Fig. 3 (e.g., spots, stripes, mixtures) evolve into synchronized states across layers. The parameter values are the same as Fig. 3.

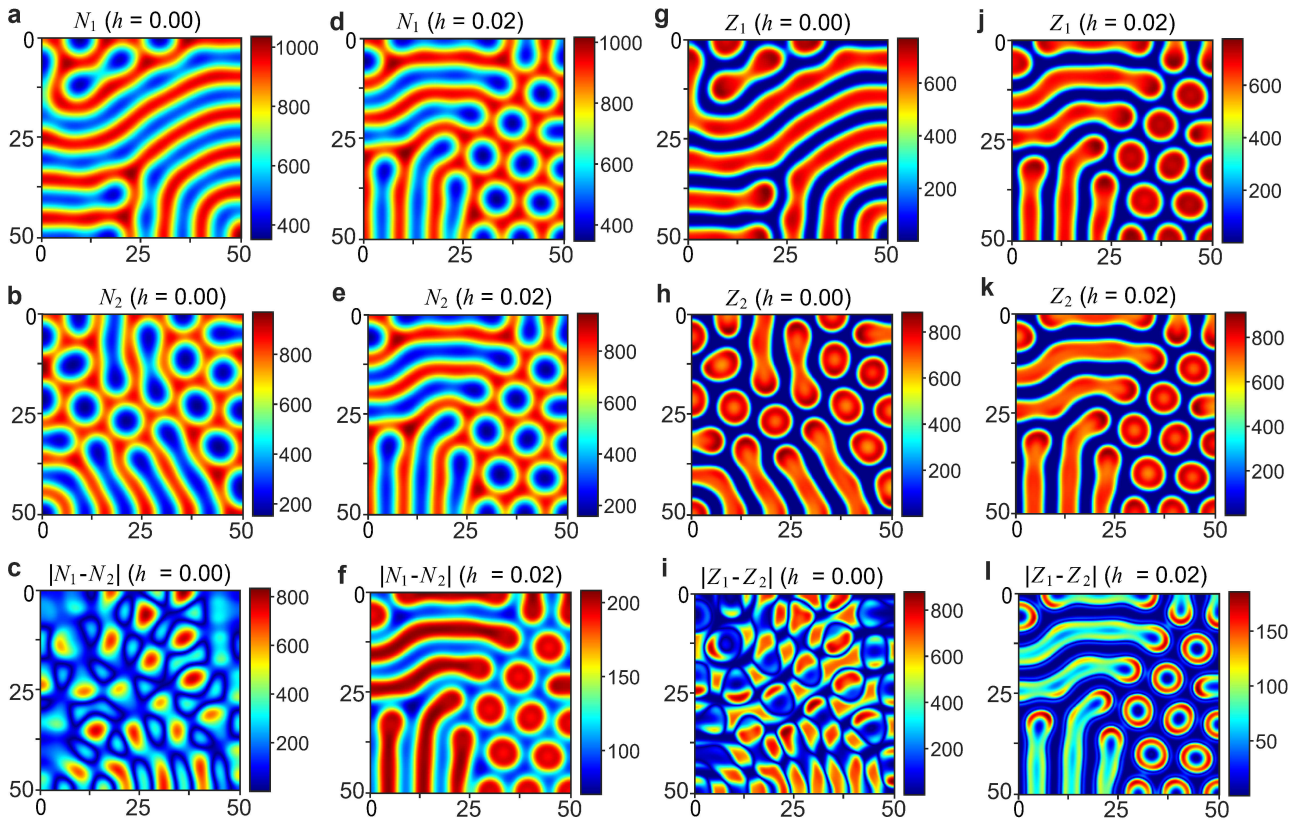


Figure S3: Visual comparison of self-organized patterns and their synchronization errors for non-coupled (Fig. S3) and coupled (Fig. S3) systems. (a-l) For the non-coupled system ($h = 0$): (a-b, g-h) self-organized patterns, (c, i) pattern of the synchronization error, which exhibits a structure distinctly different from (a-b, g-h). (d-e, j-k) For the coupled system ($h = 0.02$): (d-e) synchronized patterns, (f, l) pattern of the synchronization error, which maintains structural similarity to (d-e, j-k). The parameter values are the same as Fig. 5.

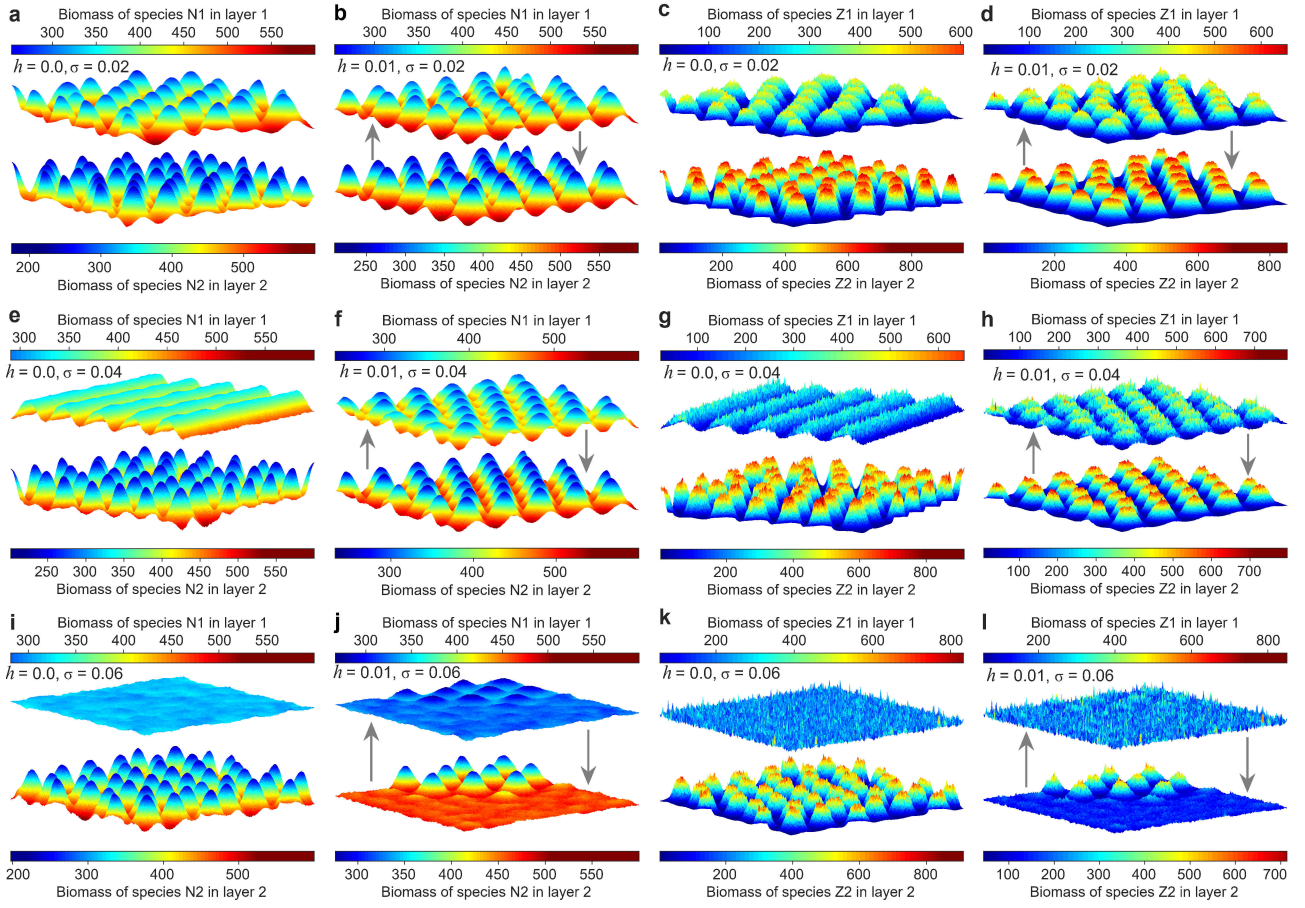


Figure S4: Effect of stochasticity on spotted pattern structures. (a, c, e, g, i, k) Without coupling, increasing noise intensity affects the upper layer more than the lower layer: the upper-layer pattern transitions from spots to stripes and eventually vanishes, while the lower layer maintains its spotted structure. (b, d, f, h, j, l) With coupling, the system exhibits robustness to stochastic fluctuations, preserving the spotted structure in both layers until the noise intensity exceeds a critical threshold, beyond which the spatial patterns collapse. The parameter values are the same as Fig. 6.

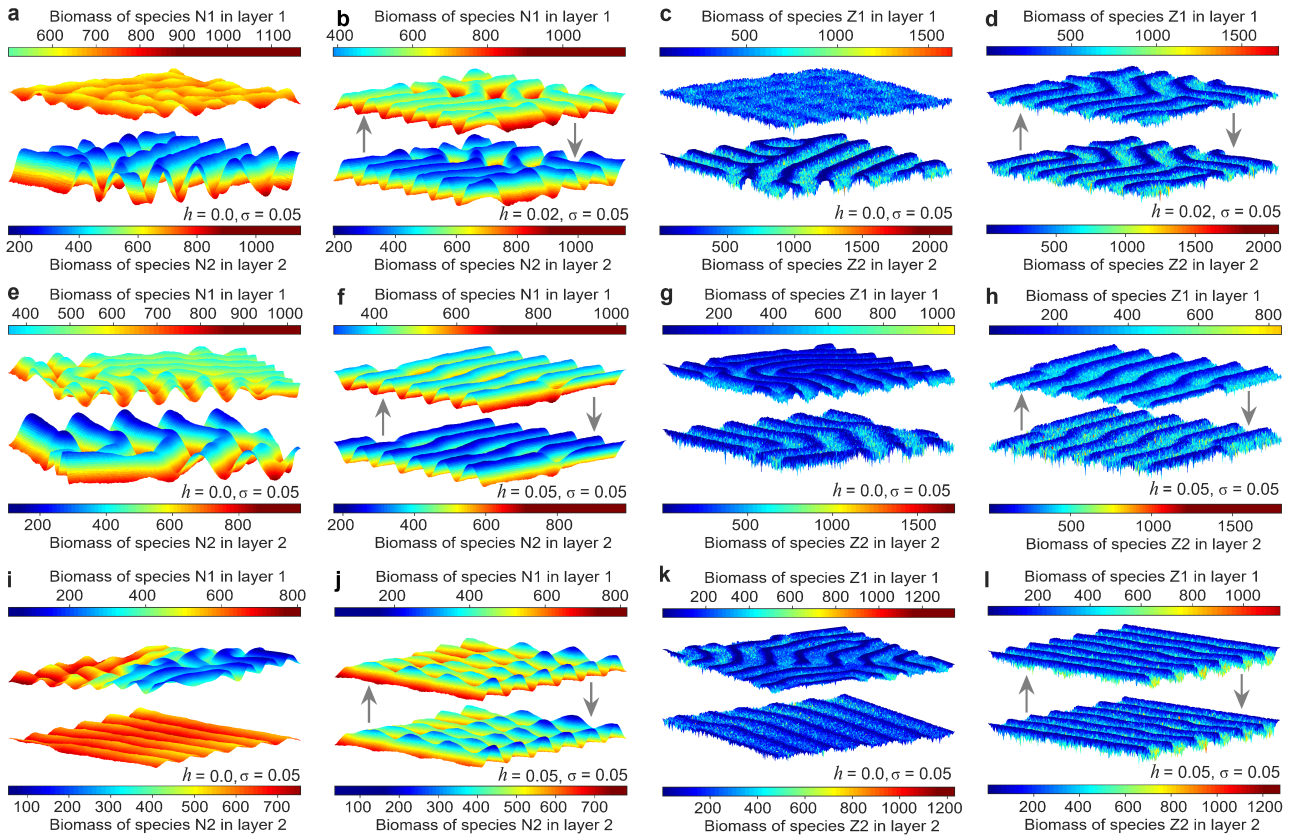


Figure S5: Robust synchronization patterns by coupling in a stochastic environment. (a, c, e, g, i, k) Without coupling, the two layers maintain distinct and independent spatial patterns in the presence of noise. (b, d, f, h, j, l) With coupling introduced, the initially different patterns achieve a robust synchronized state, demonstrating that coupling can overcome both initial heterogeneity and stochastic perturbations to establish synchronous dynamics. The parameter values are the same as Fig. 7.